Penerbit Akademia Baru

Journal of Advanced Research in Micro and Nano Engineering

Journal homepage:
https://www.akademiabaru.com/submit/index.php/armne/index
ISSN: 2756-8210

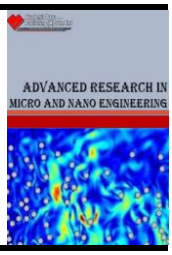

Photocatalytic Degradation of Methylene Blue and Methyl Orange Dye by Using the Core-Shell Structure of Fe_3O_4@ZnS Nanoparticles

Benazir S Pirjade[1], Shivaji Dinkar Jadhav[1], Israr Ahmad Shaikh[2], Sher Afghan Khan[3,*]

[1] Bharati Vidyapeeth (Deemed to be University) Yashwantrao Mohite College of Arts, Science and Commerce, Pune-411038, India
[2] Bharati Vidyapeeth (Deemed to be University) College of Engineering Pune-411043, India
[3] Department of Mechanical Engineering, Faculty of Engineering, IIUM, Gombak Campus, Kuala Lumpur, Malaysia

ARTICLE INFO

Article history:
Received 5 December 2023
Received in revised form 17 January 2024
Accepted 25 February 2024
Available online 30 March 2024

Keywords:
Photocatalysis; degradation; dye removal; core-shell nanoparticles; water treatment

ABSTRACT

A straightforward and highly efficient method was developed for the synthesis of Fe_3O_4@ZnS core-shell nanoparticles (NPs). These synthesized materials were subsequently utilized for the photocatalytic degradation of methylene blue (MB) and methyl orange (MO) dyes. The structural characteristics of the prepared sample were meticulously investigated through X-ray diffraction (XRD) and field-effect scanning electron microscopy (FESEM). The XRD analysis confirmed the crystalline phase formation in the Fe_3O_4 nanoparticles, while a study in the Vibrating Sample Magnetometer (VSM) mode emphasized their strong ferromagnetic behavior. The degradation of dyes was comprehensively studied using UV-Vis analyses, taking into account factors such as pH and initial dye concentration in the decolorization process. The synthesized Fe_3O_4@ZnS core-shell nanostructure underwent thorough characterization using XRD, UV-Vis spectroscopy, SEM, Fourier-transform infrared spectroscopy (FT-IR), and VSM mode in PPMS. Furthermore, the reusability of the catalyst was explored, yielding promising results. The findings demonstrated the efficient photocatalytic degradation of MB and MO dyes under UV-visible irradiation, achieving significant results within 30-minute intervals.

1. Introduction

The presence of synthetic dyes in industrial wastewater poses a formidable environmental challenge, demanding innovative solutions for their efficient removal. Photocatalysis has emerged as a promising technology for degrading these persistent organic pollutants, with core-shell nanostructures offering a unique avenue for enhanced catalytic performance [1]. This study delves into the photocatalytic degradation of two prominent synthetic dyes, MB and Methylene Orange (MO), employing a core-shell Nano composite composed of Fe_3O_4 as the core and ZnS as the shell (Fe_3O_4@ZnS).

The significance of core-shell nanostructures in environmental remediation has prompted diverse synthesis techniques to create these advanced materials [2].

* *Corresponding author.*
E-mail address: sakhan@iium.edu.my

https://doi.org/10.37934/armne.17.1.4255

Liu and their team [3] have pioneered the application of double-shelled hollow structures made up of γ-Fe_2O_3/ZnO for the removal of a variety of dyes, such as MB, Rhodamine B (RhB), and MO.

Xie *et al.,* [4] investigated the degradation of pentachlorophenol using different mole ratios of α-Fe_2O_3/ZnO photocatalysts and showcased their effectiveness. In a separate study, Sanad and their collaborators [5] utilized ZnS-ZnO nanocomposites to efficiently eliminate dyes like MB and eosin.

Hitkari *et al.,* [6] concurrently delved into the study of the photocatalytic potential of ZnO/ZnS and ZnO/ZnS/α-Fe_2O_3 nanocomposites for the degradation of MO. In a separate investigation, the Xu research group [7] presented a core-shell heterostructure, Fe_3O_4@SiO_2@ZnO/ZnS, aimed at effectively eliminating organic pollutants like TC, MB, and RhB through photocatalysis.

In this context, introducing a novel magnetic nanocomposite with a modified core-shell structure, incorporating zinc sulfide (ZnS) and iron oxide (Fe_3O_4). This nanocatalyst offers several benefits, such as stability, straightforward synthesis, cost-effectiveness, and environmental compatibility [8]. Rigorously evaluating the efficacy of this novel nanocatalyst for the removal of dyes, not only in synthetic wastewater but also in real-world scenarios using wastewater samples obtained from the colored wastewater of the textile factory [9].

One remarkable observation is the nanocatalyst's proficiency in both the ultraviolet (UV) and visible regions, with exceptional efficiency particularly demonstrated in the UV spectrum. Moreover, the utilization of a UV and visible lamp as the light source enhances the cost-effectiveness, durability, and overall efficiency of the photocatalytic process in removing organic pollutants compared to alternative light sources available in the market [10].

This study thus sheds light on the potential of the Fe_3O_4@ZnS core-shell nanocomposite as an eco-friendly and efficient solution for addressing dye pollution, further advancing the principles of green chemistry and contributing to the preservation of precious water resources and ecosystems.

2. Methodology

2.1 Materials

All chemicals were used in analytical grade without any further purification.

Ferric chloride ($FeCl_3.6H_2O$), ferrous chloride ($FeCl_2.4H_2O$), and sodium hydroxide (NaOH). Sodium sulphide (Na_2S), zinc sulphide ($ZnSO_4.H_2O$).

2.2 Synthesis of Fe_3O_4@ZnS Core-Shell Nanoparticles

For the synthesis of Fe_3O_4@ZnS core-shell nanostructures, initially, the Fe_3O_4 nanoparticles were synthesized by co-precipitation of $FeCl_3.6H_2O$ (ferric chloride) and $FeCl_2.4H2O$ (ferrous Chloride) where the solution was made in 50 ml double distilled water with a molar ratio of 2:1, respectively. NaOH (0.8M) solution prepared in 50 ml double distilled water was next added dropwise with the help of an addition funnel with stirring for 2 hrs. The capping agent, 1 gm PVP, is added to the reaction at a suitable stage of the reaction. In the second stage, an aqueous solution of ZnS (1:1M ratio of Zn ($ZnSO_4$) to S(Na_2S)) was added dropwise in the colloid having Fe_3O_4 nanoparticles to obtain the ZnS shell on the Fe_3O_4 core. The colloid formed was then removed and centrifuged to collect the sample. After this, it was redispersed in double distilled water with the help of a sonic bath. The solution was further centrifuged 2-3 times to remove unreacted reagents from the solvent. In the end, the sample was collected and dried overnight and crushed to obtain it in powder form.

Fe_3O_4@ZnS nanoparticles with a core-shell structure were successfully synthesized. This makes the nanoparticles suitable for a range of applications and additional characterization.

2.3 Characterization

A variety of characterization techniques were used to conduct a thorough examination of the structural and morphological characteristics of the core-shell Fe_3O_4@ZnS nanoparticles intended for the elimination of MB and MO dyes [11]. Using a JEOL-JDX–8030 apparatus and 40 kV and 30 mA as operating conditions, X-ray diffraction (XRD) analysis was used to perform the structural evaluation. The examination of the intrinsic crystal structures in the produced nanoparticles was made possible by this technique. The morphological characteristics of the core-shell nanoparticles were thoroughly examined using field-emission scanning electron microscopy (FE-SEM). This procedure allowed for a thorough analysis of the physical properties and dispersion of the nanoparticles by carefully mounting the samples on both Si substrates and lacey carbon Cu grids.

A double-beam UV-Vis spectrophotometer was used to assess the optical characteristics and obtain important information about the UV-Vis diffuse reflectance and absorption spectra. The optical characteristics of the nanoparticles, which are essential to their photocatalytic effectiveness in the degradation of dyes like MB and MO, were clarified with the use of this spectroscopic investigation. Together, these thorough characterization techniques advance our understanding of the structural, morphological, and optical characteristics of the core-shell Fe_3O_4@ZnS nanoparticles. Such understanding is necessary for their effective use in the removal of dyes from wastewater.

2.4 Photocatalytic Degradation

The degradation of MB and MO dye was carefully studied to determine the photocatalytic activity of Fe2O4@ZnS nanoparticles under irradiation conditions as UV (27 watts).

This experiment was conducted in a solution comprising 80 mg Fe_3O_4@ZnS nanoparticle catalyst carefully mixed with 5 mg per ml of MB dye and MO, assuring extensive dispersion through constant stirring. Approximately 4ml of the reaction mixture was painstakingly removed at predetermined intervals of 0, 30, 60, and 90 minutes. These extracted materials were then put through a demanding centrifugation procedure that involved spinning at 5,000 revolutions per minute for 20 minutes.

A UV-visible spectrophotometer was used to examine the MB and MO dye degradation with extreme care and precision, giving a thorough evaluation of the changes in dye concentration over time and shedding light on the efficiency of the photocatalytic process under both ultraviolet and visible irradiation conditions.

2.5 X-Ray Diffraction Analysis (XRD)

To clarify the crystalline structure of the Fe_3O_4@ZnS core-shell nanoparticles, X-ray diffraction (XRD) research was carried out. The XRD pattern (Figure 1) showed different peaks at different angles, which indicates that the material has different crystal planes. In particular, the cubic phase of ZnS (jcpds file 12-0688) was identified at angles of 28.92° (111), 47.62° (220), and 56.64° (311). Furthermore, peaks corresponding to the cubic phase of Fe_3O_4 (JCPDSfile 19-0629) were observed at 30° (220), 35^0(311), 43.28° (400), 55.15° (422), 57.3^0(511) and 64° (440).

The Debye-Scherrer Eq. (1) was employed to calculate the crystallite size of ZnS NP on the (311) plane, yielding a size of 2.6 nm. The crystallite size determination was conducted using the formula

$$D = \frac{k\lambda}{\beta} * cos\ (\theta) \quad (1)$$

where:

- D stands for the size of the crystallite.
- The form factor, or K, is 0.9 for spherical particles.
- λ, or 1.54 Å, is the wavelength of X-rays.
- β is the tallest peak's full width at half-maxima (FWHM) in radians.

Additionally, the XRD analysis confirmed the presence of cubic ZnS in the photocatalyst structure. These XRD results provide valuable insights into the crystalline nature and structural properties of the Fe_3O_4@ZnS core-shell nanoparticles.

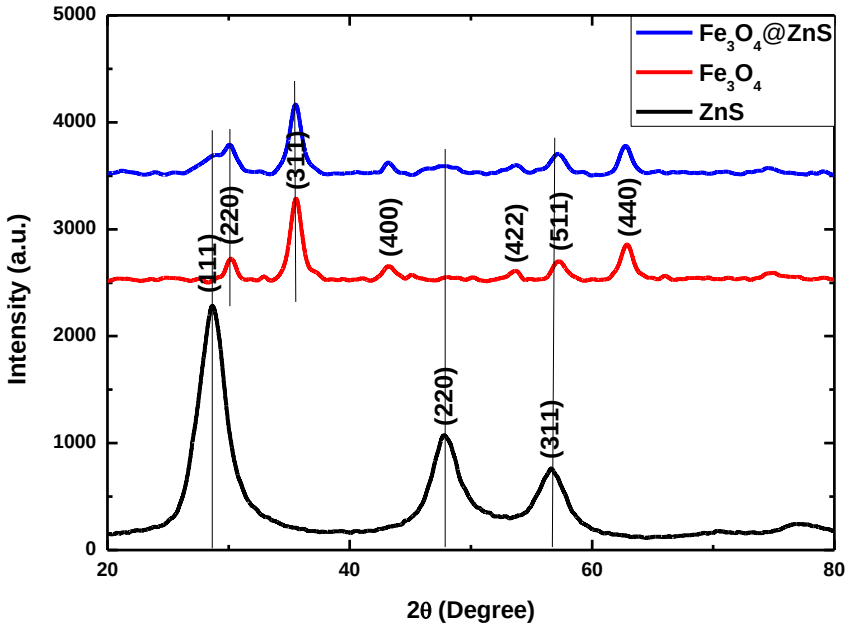

Fig. 1. XRD of Fe_3O_4, ZnS and Fe_3O_4@ZnS for dye degradation

2.6 Field Effect Scanning Electron Microscope (FESEM)

An analysis was conducted to examine the particle size distribution of the Fe_3O_4@ZnS photocatalyst, utilizing Field Effect Scanning Electron Microscopy (FESEM) to comprehend the dimensions and structure of the particles [11]. The FESEM examination revealed spherical particles with a consistent distribution in the Fe_3O_4@ZnS, displaying an average size ranging between 6 to 8 nm (Figure 2(a) and 2(b)). This spherical shape and even distribution of particles were predominantly maintained even after the attachment of the ZnS shell onto the Fe_3O_4 core. Further SEM images were taken to enable a comprehensive comparison of the synthesized photocatalysts, specifically focusing on the Fe_3O_4@ZnS samples [12,13]. These images reaffirmed the uniform distribution of nanoparticles in both samples, portraying a spherical morphology [14]. These microscopic evaluations provide crucial insights into the structural attributes and size distribution of the Fe_3O_4@ZnS photocatalyst.

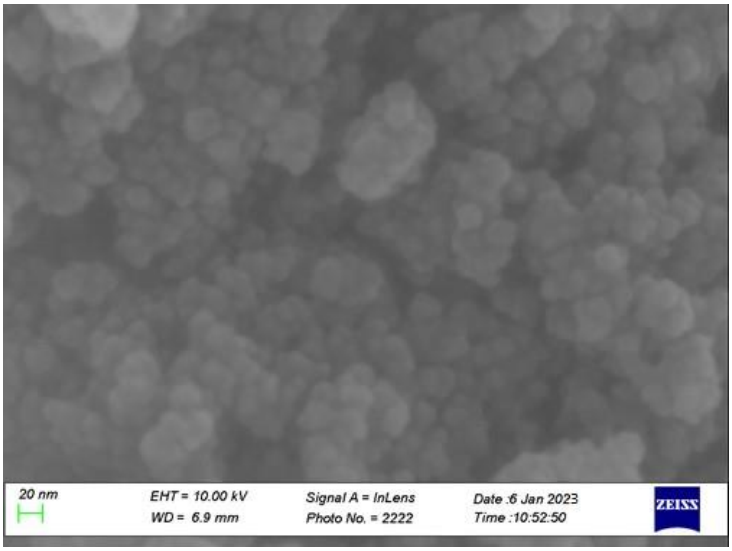

(a)

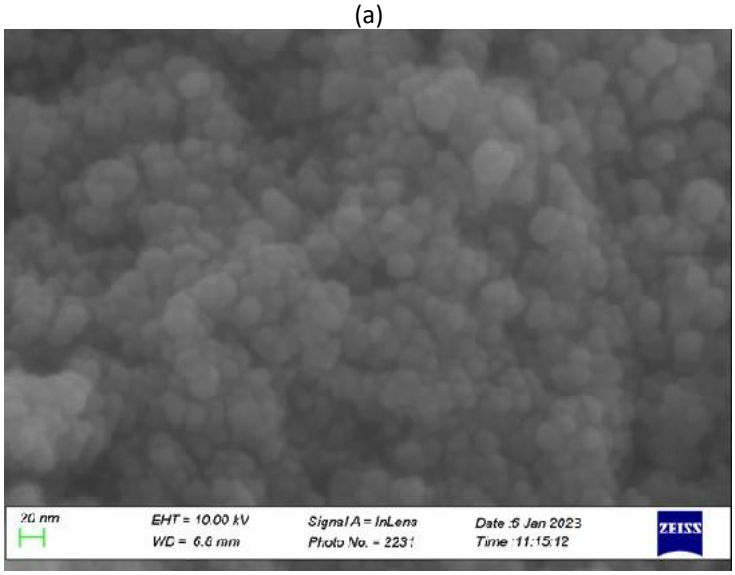

(b)

Fig. 2. (a, b) SEM images of Fe_3O_4@ZnS nanoparticles

2.7 PPMs in VSM Mode

PPMS in VSM (Vibrating Sample Magnetometer) measurements could be conducted to determine the magnetic properties of the Fe_3O_4@ZnS nanoparticles at room temperature, including their magnetization behavior, saturation magnetization, and magnetic hysteresis as shown in Figure 3. PPMS in VSM can be used to investigate how the core-shell structure of Fe_3O_4@ZnS nanoparticles affects their magnetic behavior, providing insights into their potential applications in magnetic separation and drug delivery systems. PPMS in VSM measurements can help in studying how the nanoparticle size influences their magnetic properties, revealing any size-dependent magnetism that could be useful in various nanomaterial applications [15]. Figure 3 shows the magnetization saturation value is 54 emu/g for Fe_3O_4, which is reduced to 36 emu/g for Fe_3O_4 @Zns. The magnetization saturation value is reduced because of the formation of a non-magnetic layer on the magnetic nanoparticle. The magnetic hysteresis loop displays no remanence or coercivity in the experiment conditions, which suggests that the magnetic nanoparticles exhibit magnetic character.

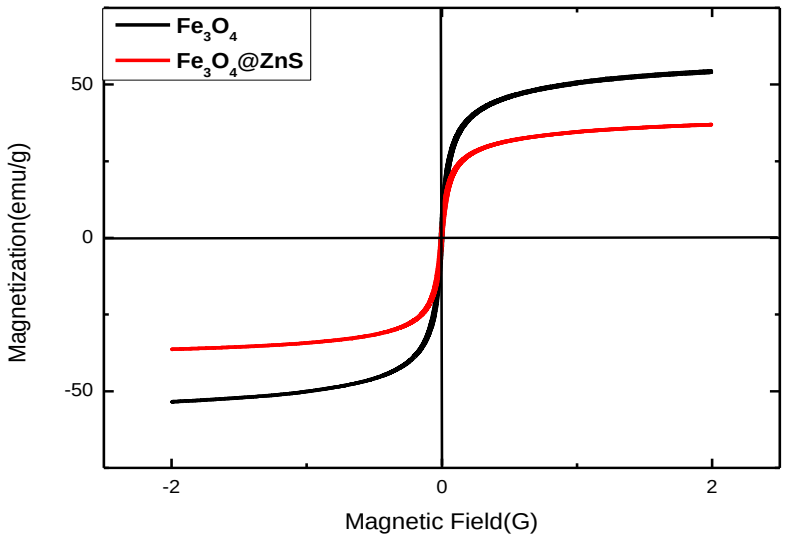

Fig. 3. PPMS in VSM mode of Fe_3O_4 and Fe_3O_4@ZnS nanoparticles

2.8 Fourier Transform Infrared Spectroscopy (FTIR)

The FTIR spectra provided more evidence of the core-shell structure's effective formation by revealing discrete peaks that matched the unique characteristics of both the ZnS and Fe_3O_4 elements. The integrity of the composite material was highlighted by this research, which supported the idea that the core-shell structure maintained the chemical properties of both Fe_3O_4 and ZnS. Moreover, the identification of putative functional groups or surface modifications that might be important for the photocatalytic destruction of dyes was made possible by FTIR spectroscopy [16,17]. Any modifications or shifts in peak locations associated with the photocatalytic reactions could be observed by examining the FTIR spectra. The IR spectrum of Fe_3O_4@ZnS (Figure 4) shows the stretching vibrations of 610.1 for ZnS and 617 for Fe-O. The hydroxyl groups on the surface of Fe_3O_4 NPs and water molecules are associated with the stretching vibrations at 3415.5 and 3475.1 cm^{-1}, while the OH bending frequency is shown at 1618.5 cm^{-1}.

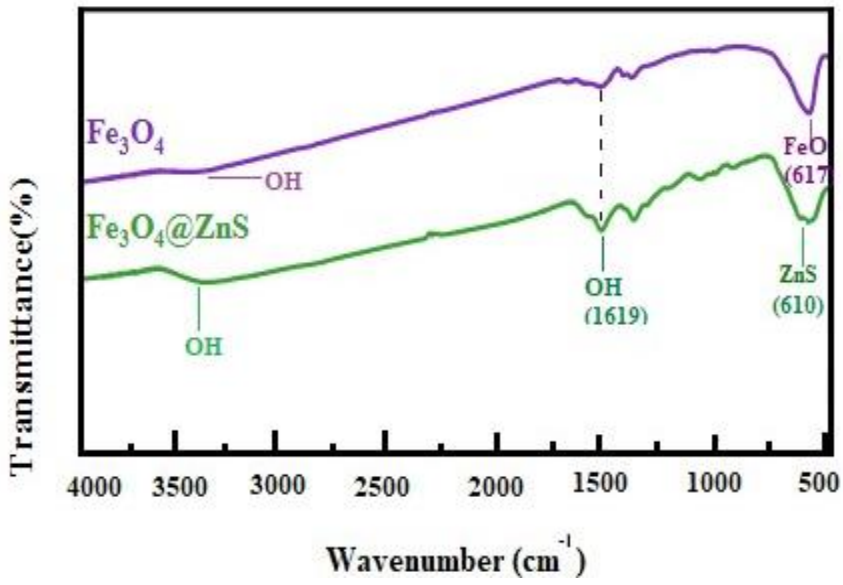

Fig. 4. FTIR analysis of Fe_3O_4@ZnS nanoparticles

3. Results and Discussion

3.1 Mechanism of Photocatalytic Degradation

The photocatalytic degradation process of MO and MB dyes using Fe_3O_4@ZnS core-shell nanoparticles are elucidated through Eq. (4)–(6). When subjected to photon irradiation, the core-shell structure of Fe_3O_4@ZnS facilitates the creation of electrons and holes. Electron transfer occurs from the valence band (VB) of the photocatalyst, while hole transfer takes place from the conduction band (CB) of the photocatalyst.

$$L_n\left(\frac{A_t}{A_0}\right) = l_n\left(\frac{C_t}{C_0}\right) = -k_{app}^t \quad (2)$$

$$ZnS + hv \rightarrow h^+ + e \quad (3)$$

$$OH^- + h^+ \rightarrow OH \quad (4)$$

$$H_2O + h^+ \rightarrow +OH + H^+ \quad (5)$$

$$O_2 + e^- \rightarrow O_2^- + H^+ \rightarrow HO_2 \quad (6)$$

The core-shell structure serves as a fundamental facilitator and enhancer of photocatalysis, playing a pivotal role in multiple applications. This distinct architecture instigates and sustains crucial oxidation and reduction reactions occurring on the surface of Fe_3O_4@ZnS nanoparticles. These processes involve adsorbed water and hydroxyl anions, which significantly contribute to the generation of essential hydroxyl radicals (•OH) crucial for the decomposition of organic compounds (Figure 5).

A variety of active species, including •OH, O_2•, HO_2•, h^+, and e^-, are involved in the breakdown of dyes and organic contaminants within the field of photocatalysis. Together, these reactive species work to break down complex molecules, making wastewater treatment and pollution remediation more efficient and environmentally benign [18,19].

The core-shell structure of Fe3O4@ZnS also guarantees effective charge separation and prevents electron and hole recombination. Important reactive species, including H^+, O_2•, OH_2•, and •OH, are essential for catalyzing redox processes and breaking down MB and MO dye into products like CO_2, H_2O, and mineral ions. Consequently, the color intensity of the MB and MO dyes decreases because of the disintegration of their aromatic rings.

Fe_3O_4@ZnS is most effective as a photocatalyst in the UV range, as Table 1 illustrates. Fe_3O_4@ZnS is active in the UV spectrum, however, it performs well in the UV spectrum, and its decolorization efficiency is relatively lower.

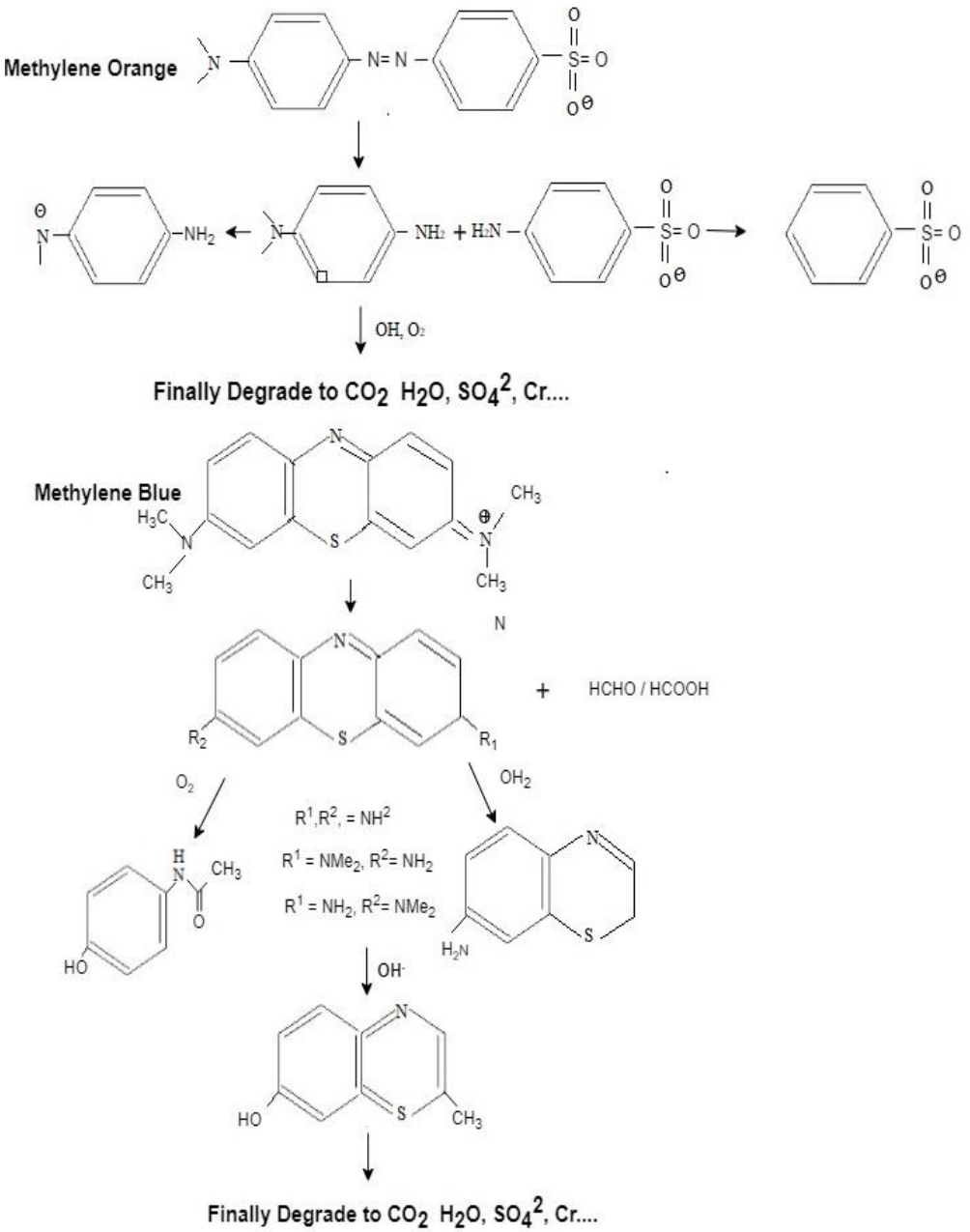

Fig. 5. Compounds of MO and MB photocatalytic degradation

3.2 Calculation of Degradation Rate

Using Fe_3O_4@ZnS as a crucial component, the main goal of this study was to examine how MO and MB decolorize when exposed to UV light. The decolorization tests in the first phase lasted 30 minutes, and the MB and MO dyes showed a little decrease as a result.

The focus shifted to assessing the removal of the dyes MB and MO under UV light conditions with a particular UV light source. After the designated amount of time for irradiation, the catalyst was successfully separated from the solution with the aid of an external magnet, and a precise 2-milliliter sample of the dye solution was taken for examination.

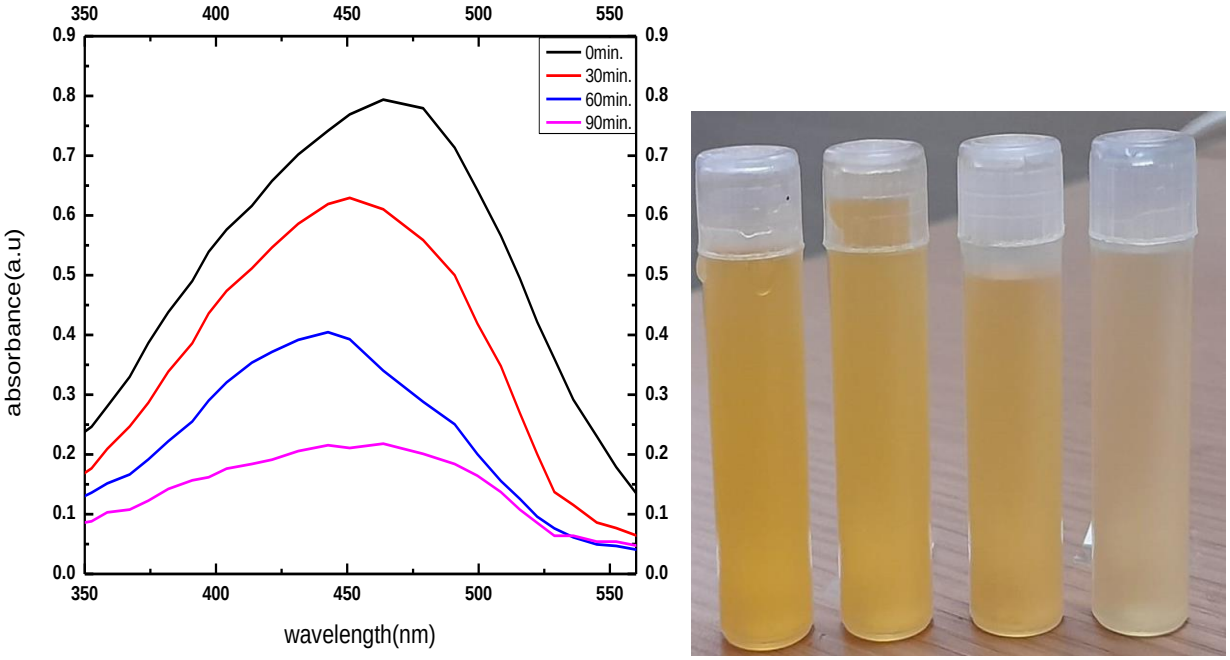

Fig. 6. Photocatalytic degradation of MO dye

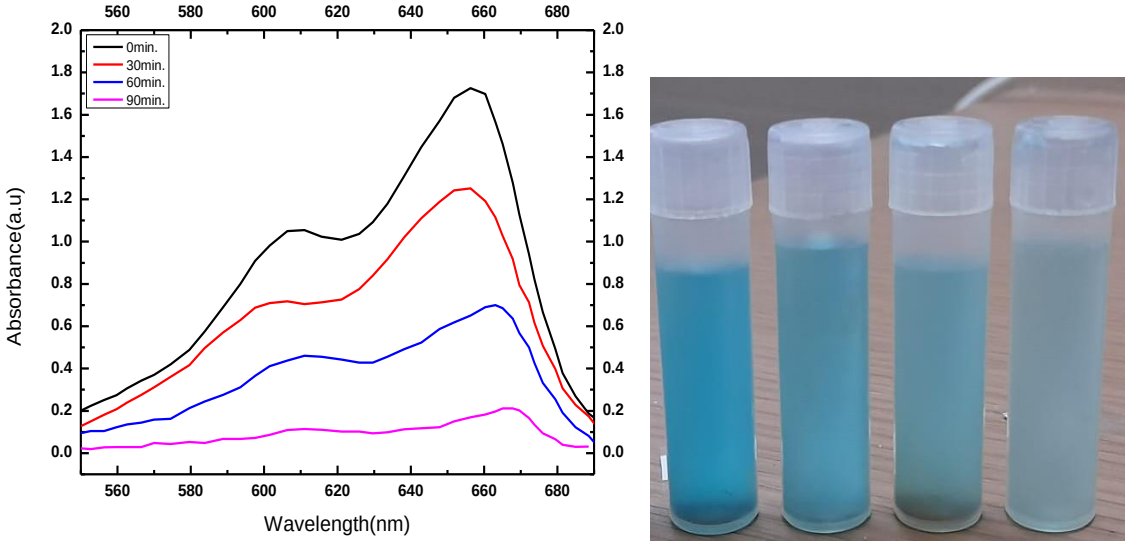

Fig. 7. Photocatalytic degradation of MB dye

This study used a UV-Vis spectrophotometer to examine the treated effluent to determine how successful the dye removal procedure was (Figures 6 and 7). By applying a certain formula to measure the color removal efficiency, we were able to obtain a thorough grasp of Fe_3O_4@ZnS's effectiveness and performance in the decolorization of these dyes.

$$Removal(\%) = \left(A_0 - \frac{A_t}{A_0}\right) * 100 \quad (7)$$

In this case, A_0 denotes the dye solution's start adsorption at time t = 0, and A_t denotes the sample's adsorption at the end time, t. With Fe_3O_4@ZnS present, the dyes MO and MB demonstrated exceptional performance. MO and MB were found to have photocatalytic dye removal (Figure 8)

rates of 74% and 87% under UV light, respectively. These outcomes were obtained with a 30-minute testing period and a catalyst amount of 0.08 g.

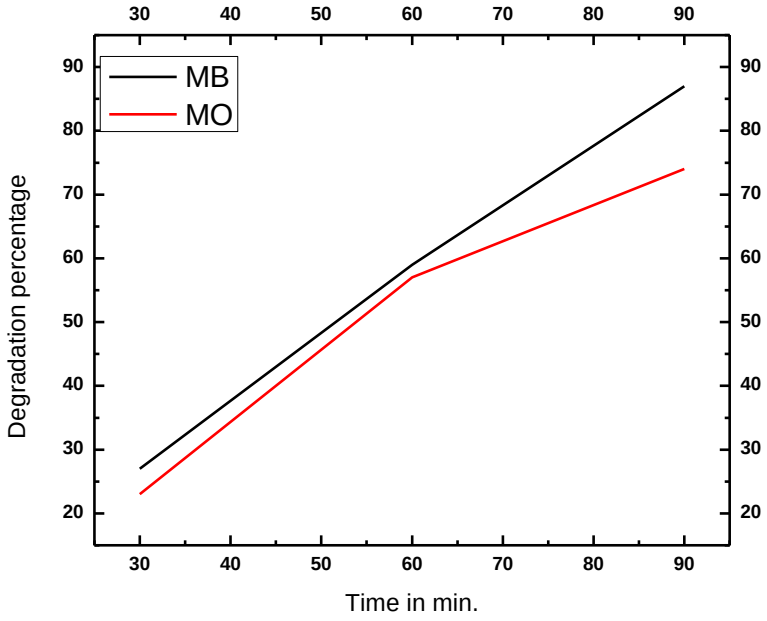

Fig. 8. Percentage degradation

By tracking each compound's unique maximum absorption wavelength (λ max), this study examined the rates of photocatalytic dye removal in aqueous solutions of MO and MB in greater detail (Figure 9). The highest absorption for MO was observed at 466 nm, whereas MB displayed its peak absorption at 664 nm. To ensure the reliability and consistency of our findings, we conducted four repeated tests under ideal conditions to assess the repeatability of dye removal responses. Remarkably, both MO and MB displayed predictable and repeatable degradation patterns, with consistent dye removal efficiencies sustained at 74% and 87%, respectively, throughout these four repetitions.

In this analysis of dye degradation kinetics, here employing the pseudo-first-order kinetics model and calculated the rate constants using Eq. (2). In this equation, A0 denotes the initial absorbance of the organic dye, while 'At' represents the absorbance of the organic dye at time t. The determined rate constants for dye removal, focusing on MO and MB, were found to be 0.0109 and 0.01298 min^{-1}, respectively. These findings confirm that the photocatalytic removal process for both MO and MB follows a first-order kinetics equation.

Table 1
The rate constant for MB and MO

Time	The rate constant (k) for MB	The rate constant (k) for MO
30	0.01079	0.0245
60	0.000189	0.0057
90	0.002003	0.002522
Mean	0.01298	0.0109

Additionally, a study was carried out to investigate the impact of varying the quantity of aqueous dye solutions on the extent of dye removal when employing the photocatalyst in the presence of UV light. Table 2 provides a detailed summary of the dye removal evaluation results at different MB and MO concentrations.

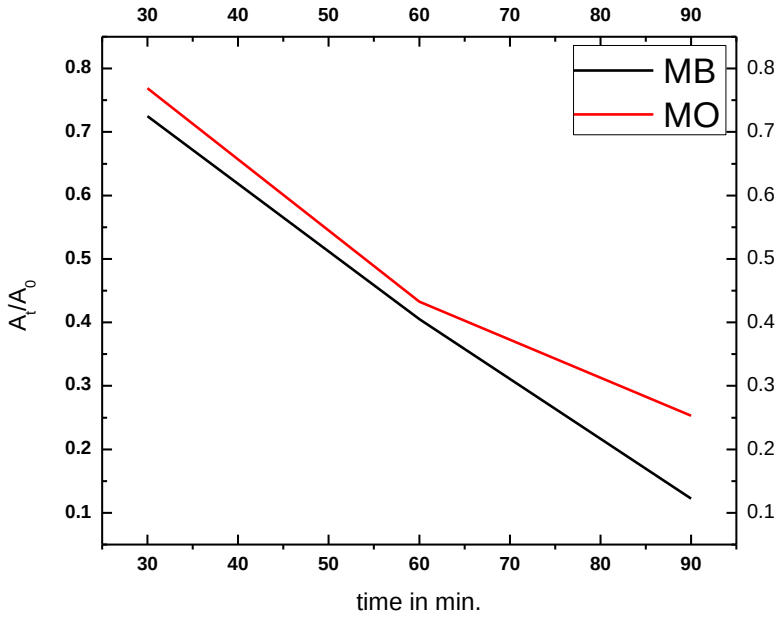

(a)

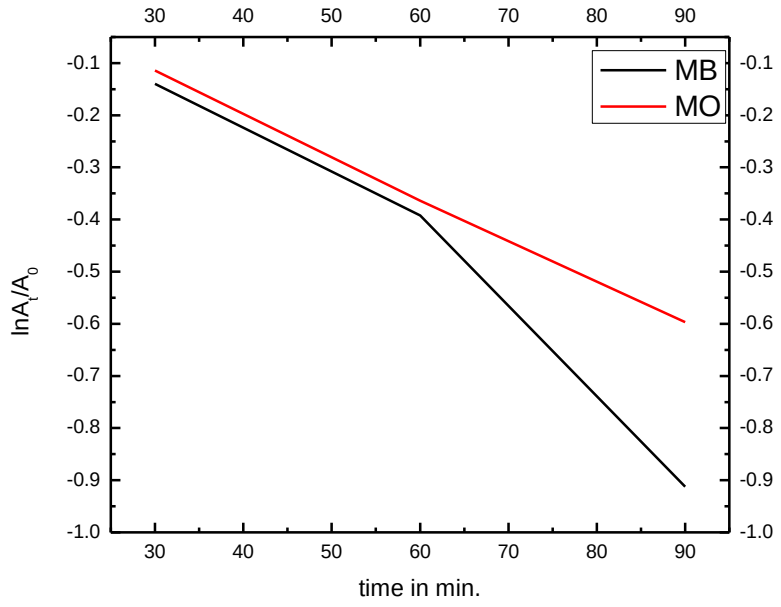

(b)

Fig. 9. First-order kinetic diagram for photocatalytic dye removal of MB and MO dye in the presence of Fe_3O_4@ZnS

3.3 The Influence of pH on the Dye Removal Process

The photocatalytic elimination process is significantly impacted by the pH of the solution. Therefore, the study examined how MO and MB degraded in the presence of UV light at different pH values, namely 3, 5, 8, and 11. Table 1 summarises the results of the photocatalytic dye removal tests using Fe_3O_4@ZnS under UV light for both MO and MB dyes.

The adsorption of dye molecules onto the surface of the photocatalyst is the first step in most photocatalytic dye removal methods (Figure 10). This is followed by the destruction of these molecules when exposed to light. The study investigated the elimination of MO dye under varying pH circumstances. The results showed that the most significant degradation rate, which was 74%,

outperformed the results at other pH levels. The unique properties of the dye and the photocatalyst's surface charge are responsible for this result.

MO, an anionic azo dye, has a lower negative charge than the photocatalyst. Consequently, an electrostatic repulsion effect happens when the dye sticks to the surface of the photocatalyst. It's interesting to note that, even with a lower negative surface charge (-2.5 mV), MO can be removed from the solution more successfully at pH 3 than at pH 5 or 8. This surprising result can be explained by the fact that even when the negative surface charge decreases, there is less electrostatic repulsion at pH 3, which causes a larger degree of dye degradation.

On the other hand, at pH values of 3, 5, and 8, the surface of the photocatalyst retains a negative charge since MB is a cationic dye. To be more precise, at pH 8, the surface of the photocatalyst has a greater density of negative charges, which increases electrostatic attraction and improves dye absorption. As a result, the rate of dye degradation increases; MB obtains an 87% clearance rate at pH 8.

Interestingly, the photocatalyst's increased negative surface charge between pH 8 and pH 11 is responsible for the fastest rate of MB degradation that is seen at alkaline pH levels. Zeta potential measurements show that the photocatalyst surface has a greater negative charge at higher pH levels, which speeds up dye absorption and eventual degradation.

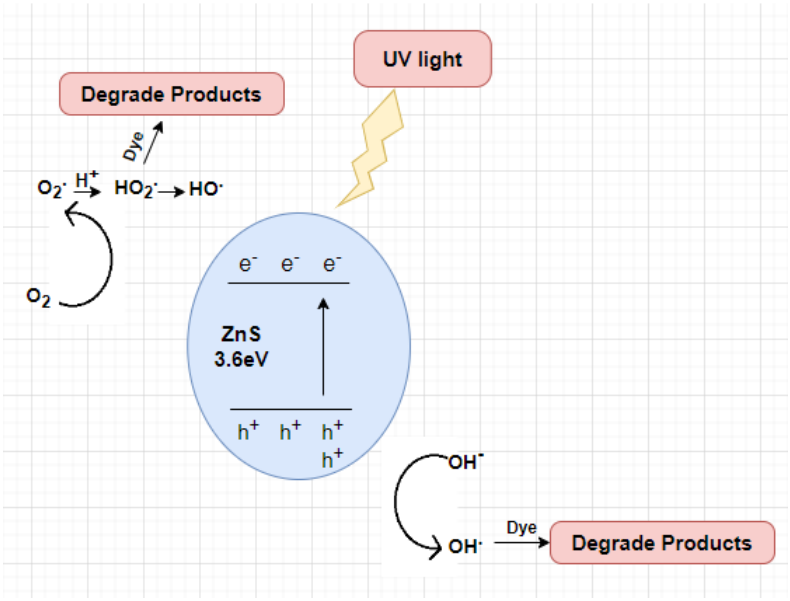

Fig. 10. Photocatalytic degradation of organic dyes in the presence of Fe_3O_4@ZnS

Table 2
The impact of raising MO and MB concentrations on dye removal effectiveness

Sr. No.	Nanoparticle	Dye removal (%)	Dye	Concentration (ppm)	Light
1	Fe_3O_4@ZnS	74	MO	10	UV
2	Fe_3O_4@ZnS	72.5	MO	15	UV
3	Fe_3O_4@ZnS	71.6	MO	20	UV
4	Fe_3O_4@ZnS	70	MO	50	UV
5	Fe_3O_4@ZnS	87	MB	10	UV
6	Fe_3O_4@ZnS	85.6	MB	15	UV
7	Fe_3O_4@ZnS	83.5	MB	20	UV
8	Fe_3O_4@ZnS	80	MB	50	UV

3.4 The Capacity to Reuse the Photocatalyst

After a thorough analysis of multiple variables, such as the amount of photocatalyst, dye concentration, light source, and pH, a reusability assessment of the photocatalyst was also carried out [20]. Under UV light for up to five cycles, the reusability of Fe_3O_4@ZnS in aqueous solutions containing MO and MB (at a 10 ppm concentration) was examined. The photocatalyst's efficiency dropped by 4% after five consecutive applications, most likely as a result of dye accumulation that obstructed the active sites on the surface. An ICP-OES analysis was carried out to obtain an accurate understanding of the quantity of ZnS attached to the surface of the nanocomposite [21]. After careful computations, the analysis's findings showed that there was 6.45 mmol of zinc sulfide—or 23.75% of zinc—for each gram of photocatalyst.

4. Conclusion

Modern treatment technologies are receiving more attention as a result of the increasing prevalence of new pollutants in water, which highlights the shortcomings of traditional wastewater treatment techniques. These cutting-edge techniques include the application of novel techniques such as biological treatments, photocatalytic reactions, enhanced biodegradability, and advanced oxidation processes (AOPs). Of these, photocatalytic reactions and biological treatment have attracted a lot of interest because they can provide sustainable, affordable, and eco-friendly solutions. As a result, there is a growing interest in switching to ecologically friendly photocatalysts from antiquated, expensive, and environmentally unfriendly approaches. This work introduces Fe_3O_4@ZnS as a unique, reusable photocatalyst for the decolorization of dyes like MB and MO in real wastewater samples. The specifically designed magnetic nanocomposite removes dyes at rates of 87% for MB and 74% for MO in 30 to 90 minutes when exposed to UV-visible light. This synthesized photocatalyst is noteworthy for its activity in the UV light spectra, with the UV region showing the highest performance. The reproducibility of dye removal findings using Fe_3O_4@ZnS, highlighting its potential as a flexible solution, is an intriguing finding in this study. Notably, this newly developed photocatalyst has potential uses in the textile, dyeing, and other sectors, as it can effectively and environmentally remove dyes from wastewater.

References

[1] Kumari, Priyanka, Nupur Bahadur, Lingxue Kong, Luke A. O'Dell, Andrea Merenda, and Ludovic F. Dumée. "Engineering Schottky-like and heterojunction materials for enhanced photocatalysis performance–a review." *Materials Advances* 3, no. 5 (2022): 2309-2323. https://doi.org/10.1039/D1MA01062J

[2] Singh, Rimmy, and Rachna Bhateria. "Core–shell nanostructures: a simplest two-component system with enhanced properties and multiple applications." *Environmental Geochemistry and Health* 43 (2021): 2459-2482. https://doi.org/10.1007/s10653-020-00766-1

[3] Liu, Yu, Le Yu, Yong Hu, Changfa Guo, Fumin Zhang, and Xiong Wen David Lou. "A magnetically separable photocatalyst based on nest-like γ-Fe 2 O 3/ZnO double-shelled hollow structures with enhanced photocatalytic activity." *Nanoscale* 4, no. 1 (2012): 183-187. https://doi.org/10.1039/C1NR11114K

[4] Xie, Juan, Zhao Zhou, Yiwei Lian, Yongjing Hao, Pan Li, and Yu Wei. "Synthesis of α-Fe2O3/ZnO composites for photocatalytic degradation of pentachlorophenol under UV–vis light irradiation." *Ceramics International* 41, no. 2 (2015): 2622-2625. https://doi.org/10.1016/j.ceramint.2014.10.043

[5] Sanad, Mohamed Fathi, Ahmed Esmail Shalan, Shreen Magdy Bazid, and Sabah M. Abdelbasir. "Pollutant degradation of different organic dyes using the photocatalytic activity of ZnO@ ZnS nanocomposite materials." *Journal of environmental chemical engineering* 6, no. 4 (2018): 3981-3990. https://doi.org/10.1016/j.jece.2018.05.035

[6] Hitkari, Gaurav, Sandhya Singh, and Gajanan Pandey. "Photoluminescence behavior and visible light photocatalytic activity of ZnO, ZnO/ZnS and ZnO/ZnS/α-Fe2O3 nanocomposites." *Transactions of nonferrous metals society of*

China 28, no. 7 (2018): 1386-1396. https://doi.org/10.1016/S1003-6326(18)64777-6
[7] Xu, Ting, Pengfei Wang, Dandan Wang, Ke Zhao, Maobin Wei, Xiaoyan Liu, Huilian Liu et al. "Ultrasound-assisted synthesis of hyper-dispersed type-II tubular Fe3O4@ SiO2@ ZnO/ZnS core/shell heterostructure for improved visible-light photocatalysis." *Journal of Alloys and Compounds* 838 (2020): 155689. https://doi.org/10.1016/j.jallcom.2020.155689
[8] Qamar, Obaid Ali, Farrukh Jamil, Murid Hussain, Sungjun Bae, Abrar Inayat, Noor S. Shah, Ammara Waris, Parveen Akhter, Eilhann E. Kwon, and Young-Kwon Park. "Advances in synthesis of TiO2 nanoparticles and their application to biodiesel production: A review." *Chemical Engineering Journal* 460 (2023): 141734. https://doi.org/10.1016/j.cej.2023.141734
[9] Capodaglio, Andrea G. "Critical perspective on advanced treatment processes for water and wastewater: AOPs, ARPs, and AORPs." *Applied Sciences* 10, no. 13 (2020): 4549. https://doi.org/10.3390/app10134549
[10] Coha, Marco, Giulio Farinelli, Alberto Tiraferri, Marco Minella, and Davide Vione. "Advanced oxidation processes in the removal of organic substances from produced water: Potential, configurations, and research needs." *Chemical Engineering Journal* 414 (2021): 128668. https://doi.org/10.1016/j.cej.2021.128668
[11] Gopika, M. S., and S. Savitha Pillai. "Investigations of structural, morphological, and optical properties of CoS/Fe3O4 composites." *Materials Today: Proceedings* 66 (2022): 3334-3339. https://doi.org/10.1016/j.matpr.2022.06.540
[12] Choi, Young In, Seungwon Lee, Seog K. Kim, Young-Il Kim, Dae Won Cho, Mohammad Mansoob Khan, and Youngku Sohn. "Fabrication of ZnO, ZnS, Ag-ZnS, and Au-ZnS microspheres for photocatalytic activities, CO oxidation and 2-hydroxyterephthalic acid synthesis." *Journal of Alloys and Compounds* 675 (2016): 46-56. https://doi.org/10.1016/j.jallcom.2016.03.070
[13] Kalantari, Shirin, and Ali Shokuhfar. "Sonochemical synthesis of Ag doped zinc sulfide/iron oxide nanocomposites for photocatalytic and magnetic separation applications." *Optical Materials* 142 (2023): 113993. https://doi.org/10.1016/j.optmat.2023.113993
[14] Li, Dan, Wey Yang Teoh, Cordelia Selomulya, Robert C. Woodward, Paul Munroe, and Rose Amal. "Insight into microstructural and magnetic properties of flame-made γ-Fe 2 O 3 nanoparticles." *Journal of Materials Chemistry* 17, no. 46 (2007): 4876-4884. https://doi.org/10.1039/b711705a
[15] Pal, Bappaditya, and P. K. Giri. "High temperature ferromagnetism and optical properties of Co doped ZnO nanoparticles." *Journal of applied physics* 108, no. 8 (2010). https://doi.org/10.1063/1.3500380
[16] Subramaniam, M. N., P. S. Goh, N. Abdullah, W. J. Lau, B. C. Ng, and A. F. Ismail. "Adsorption and photocatalytic degradation of methylene blue using high surface area titanate nanotubes (TNT) synthesized via hydrothermal method." *Journal of Nanoparticle Research* 19 (2017): 1-13. https://doi.org/10.1007/s11051-017-3920-9
[17] Yu, Zongxue, Fei Li, Qiangbin Yang, Heng Shi, Qi Chen, and Min Xu. "Nature-mimic method to fabricate polydopamine/graphitic carbon nitride for enhancing photocatalytic degradation performance." *ACS Sustainable Chemistry & Engineering* 5, no. 9 (2017): 7840-7850. https://doi.org/10.1021/acssuschemeng.7b01313
[18] Khan, Mohammad Ehtisham, Mohammad Mansoob Khan, and Moo Hwan Cho. "CdS-graphene nanocomposite for efficient visible-light-driven photocatalytic and photoelectrochemical applications." *Journal of colloid and interface science* 482 (2016): 221-232. https://doi.org/10.1016/j.jcis.2016.07.070
[19] Soltani, Nayereh, Elias Saion, W. Mahmood Mat Yunus, Maryam Erfani, Manizheh Navasery, Ghazaleh Bahmanrokh, and Kadijeh Rezaee. "Enhancement of visible light photocatalytic activity of ZnS and CdS nanoparticles based on organic and inorganic coating." *Applied Surface Science* 290 (2014): 440-447. https://doi.org/10.1016/j.apsusc.2013.11.104
[20] Subash, B., B. Krishnakumar, M. Swaminathan, and M. Shanthi. "Highly efficient, solar active, and reusable photocatalyst: Zr-loaded Ag–ZnO for reactive red 120 dye degradation with synergistic effect and dye-sensitized mechanism." *Langmuir* 29, no. 3 (2013): 939-949. https://doi.org/10.1021/la303842c
[21] Bumajdad, Ali, Metwally Madkour, Yasser Abdel-Moneam, and Maged El-Kemary. "Nanostructured mesoporous Au/TiO 2 for photocatalytic degradation of a textile dye: the effect of size similarity of the deposited Au with that of TiO 2 pores." *Journal of Materials Science* 49 (2014): 1743-1754. https://doi.org/10.1007/s10853-013-7861-0